Article

Three-Component Power Decomposition for Polarimetric SAR Data Based on Adaptive Volume Scatter Modeling

Yi Cui [1],*, Yoshio Yamaguchi [1], Jian Yang [2], Sang-Eun Park [1], Hirokazu Kobayashi [1] and Gulab Singh [1]

[1] Faculty of Engineering, Niigata University, 8050 Ikarashi 2-no-cho, Nishi-ku, Niigata 950-2108, Japan; E-Mails: yamaguch@ie.niigata-u.ac.jp (Y.Y.); s.park@wave.ie.niigata-u.ac.jp (S.-E.P.); kobayashi@ie.niigata-u.ac.jp (H.K.); g.singh@wave.ie.niigata-u.ac.jp (G.S.)

[2] Department of Electronic Engineering, Tsinghua University, Beijing 100084, China; E-Mail: yangjian.ee@gmail.com

* Author to whom correspondence should be addressed; E-Mail: cuiyi.trea@gmail.com; Tel.: +81-25-262-7763; Fax: +81-25-262-6752.

Abstract: In this paper, the three-component power decomposition for polarimetric SAR (PolSAR) data with an adaptive volume scattering model is proposed. The volume scattering model is assumed to be reflection-symmetric but parameterized. For each image pixel, the decomposition first starts with determining the adaptive parameter based on matrix similarity metric. Then, a respective scattering power component is retrieved with the established procedure. It has been shown that the proposed method leads to complete elimination of negative powers as the result of the adaptive volume scattering model. Experiments with the PolSAR data from both the NASA/JPL (National Aeronautics and Space Administration/Jet Propulsion Laboratory) Airborne SAR (AIRSAR) and the JAXA (Japan Aerospace Exploration Agency) ALOS-PALSAR also demonstrate that the proposed method not only obtains similar/better results in vegetated areas as compared to the existing Freeman-Durden decomposition but helps to improve discrimination of the urban regions.

1. Introduction

The polarimetric synthetic aperture radar (PolSAR) data have never been so widely available to the remote sensing community as it is today, thanks to the launch of recent systems such as ALOS-PALSAR, RADARSAT-2, TerraSAR-X, *etc*. Effective and efficient interpretation of such mass amount of data thus meets its urgent need. Among the many analyzing tools, polarimetric scattering power decomposition methods [1–9] have become a popular choice because of their clear physical explanation, convenient implementation, and easy visual interpretation.

The original three-component decomposition proposed by Freeman and Durden [1] models the volume scattering as a cloud of uniformed distributed dipoles, and this leads to the use of a fixed coherency matrix. However, a practical issue associated with a fixed volume scattering model is that negative powers which are physically unacceptable may arise for the extracted surface and double-bounce scattering. Attempts have been made to correct such a problem as in [2,3]. In a more recent paper, a non-negative eigen-value constraint has been added [4]. The volume scattering power is obtained as the maximum value retaining the positive-definiteness of the remaining covariance matrix. The surface scattering and double-bounce scattering powers are thus derived through eigen-decomposition. Such treatment also produces a fourth component, called the remainder, which may not necessarily represent any known scattering mechanism. Arii *et al*. [5] take a further step in this framework by introducing an adaptive volume scattering model. The adaptive parameters are determined by minimizing the power in the covariance matrix after the volume scattering is subtracted. This method generally takes longer to process because numerical searching in the parameter space is needed.

In this paper, we modify the three-component scattering power decomposition method with an adaptive volume scattering model. The adaptive volume scattering model is proposed with three purposes. Firstly, it is to render a mathematically rigorous treatment for eliminating negative powers; secondly, it will not drastically deviate from existing physically-based models (e.g., cloud of dipoles) in vegetated areas; last, it remains easy and fast given the large dimensions of remotely sensed data. The paper is organized as follows. In Section 2, double transformation of the coherency matrix is introduced as a preprocessing step. In Section 3, the adaptive volume model is proposed together with the associated decomposition algorithm. In Section 4, experimental results with PolSAR data are presented. Finally Section 5 gives some discussion and concludes the paper.

2. Double Transformation of Coherency Matrix

In this section, we adopt the method of [6] to perform a double transformation on the coherency matrix as a preprocessing of the PolSAR data. It has been shown that this procedure helps discriminate oblique urban areas from vegetation and consequently gives a more accurate result [3,6,7]. In the following, we describe the transformation method in order to be self-contained. Some important properties of the transformed coherency matrix are also pointed out which accounts for the success of the proposed decomposition as will be explained in Section 4.

2.1. Orthogonal Transformation (Rotation) of Coherency Matrix

In this paper, the data format of the coherency matrix is dealt with. It should be noted that in the original paper by Freeman and Durden, a covariance matrix is decomposed [1]. Coherency matrix and covariance matrix are in fact equivalent to each other in the sense of linear transformation. However, the coherency matrix represents a clearer physical explanation in terms of surface and double bounce scattering. It also renders a simpler formula for orientation angle compensation as will be seen later. As a second order statistic of the polarimetric information, the coherency matrix is formed by ensemble averaging the outer-product of the Pauli vector, *i.e.*,

$$T = \begin{bmatrix} T_{11} & T_{12} & T_{13} \\ T_{12}^* & T_{22} & T_{23} \\ T_{13}^* & T_{23}^* & T_{33} \end{bmatrix} = \langle k_p k_p^H \rangle \tag{1}$$

where the superscripts * and ^{H} denote the complex conjugate and the conjugate transpose, respectively; $k_p = \frac{1}{\sqrt{2}}[S_{HH} + S_{VV}, S_{HH} - S_{VV}, 2S_{HV}]^T$ is the Pauli vector. Rotation of T by the orthogonal transformation is defined as [7]:

$$T(\theta) = R_1(\theta) T R_1^T(\theta) = \begin{bmatrix} T_{11}(\theta) & T_{12}(\theta) & T_{13}(\theta) \\ T_{12}^*(\theta) & T_{22}(\theta) & T_{23}(\theta) \\ T_{13}^*(\theta) & T_{23}^*(\theta) & T_{33}(\theta) \end{bmatrix} \tag{2}$$

where $R_1(\theta)$ is an orthogonal matrix given by:

$$R_1(\theta) = \begin{bmatrix} 1 & 0 & 0 \\ 0 & \cos 2\theta & \sin 2\theta \\ 0 & -\sin 2\theta & \cos 2\theta \end{bmatrix} \tag{3}$$

The rotation angle 2θ is derived by minimizing the $T_{33}(\theta)$ term. Specifically, according to Equations (2) and (3), $T_{33}(\theta)$ becomes:

$$T_{33}(\theta) = \frac{1}{2}(T_{22} + T_{33}) - \frac{1}{2}[(T_{22} - T_{33})\cos 4\theta + 2\mathrm{Re}(T_{23})\sin 4\theta] \tag{4}$$

Equating the derivative of $T_{33}(\theta)$ to zero yields:

$$\tan 4\theta = \frac{2\mathrm{Re}(T_{23})}{T_{22-}T_{33}} \tag{5}$$

From Equation (5) we have $\mathrm{Re}(T_{23}) = (T_{22} - T_{33})\tan 4\theta/2$. By substituting $\mathrm{Re}(T_{23})$ into Equation (4), and after some necessary simplification, $T_{33}(\theta)$ can be rewritten as:

$$T_{33}(\theta) = \frac{1}{2}\left[(T_{22} + T_{33}) - \frac{T_{22} - T_{33}}{\cos 4\theta}\right] \tag{6}$$

For minimizing $T_{33}(\theta)$, it follows from Equation (6) that $T_{22} - T_{33}$ and $\cos 4\theta$ should be of the same sign. Then according to Equation (5), we have:

$$2\theta = \frac{1}{2}\left\{\tan^{-1}\left[\frac{2\mathrm{Re}(T_{23})}{T_{22} - T_{33}}\right] + k\pi\right\} \tag{7}$$

where $k = 0$ if $T_{22} - T_{33} > 0$; and $k = 1$ if $T_{22} - T_{33} < 0$.

It is worth noting that rotating the coherency matrix by the orthogonal transformation leads to two important properties for $\boldsymbol{T}(\theta)$. Firstly, $T_{22}(\theta)$ is always larger than $T_{33}(\theta)$, *i.e.*, $T_{22}(\theta) > T_{33}(\theta)$; second, $T_{23}(\theta)$ becomes purely imaginary and $T_{23}(\theta) = j\mathrm{Im}(T_{23})$. As will be shown in Section 3, the former property is a necessary condition that guarantees non-negative powers in the decomposition results.

2.2. Unitary Transformation of Coherency Matrix

In [6], it is proposed that the matrix $\boldsymbol{T}(\theta)$ is further processed by a unitary transformation, that is:

$$\boldsymbol{T}(\varphi) = \begin{bmatrix} T_{11}(\varphi) & T_{12}(\varphi) & T_{13}(\varphi) \\ T_{12}^*(\varphi) & T_{22}(\varphi) & T_{23}(\varphi) \\ T_{13}^*(\varphi) & T_{23}^*(\varphi) & T_{33}(\varphi) \end{bmatrix} = \boldsymbol{R}_2(\varphi)\boldsymbol{T}(\theta)\boldsymbol{R}_2^H(\varphi) \tag{8}$$

where $\boldsymbol{R}_2(\varphi)$ is a unitary matrix given by

$$\boldsymbol{R}_2(\varphi) = \begin{bmatrix} 1 & 0 & 0 \\ 0 & \cos 2\varphi & j\sin 2\varphi \\ 0 & j\sin 2\varphi & \cos 2\varphi \end{bmatrix} \tag{9}$$

The rotation angle 2φ is also derived by minimizing $T_{33}(\varphi)$ and by a similar reasoning. It is:

$$2\varphi = \frac{1}{2}\tan^{-1}\left\{\frac{2\mathrm{Im}[T_{23}(\theta)]}{T_{22}(\theta) - T_{33}(\theta)}\right\} \tag{10}$$

Note that in Equation (10) $T_{22}(\theta) > T_{33}(\theta)$, as the result of the orthogonal transformation by $\boldsymbol{R}_1(\theta)$, so that no ambiguity correction is needed as in Equation (7).

In the transformed coherency matrix $\boldsymbol{T}(\varphi)$, the inequality $T_{22}(\varphi) > T_{33}(\varphi)$ still holds because of the minimization of $T_{33}(\varphi)$; in addition, it can be easily proved that the element $T_{23}(\varphi)$ is forced to be completely zero, *i.e.*, $T_{23}(\varphi) = 0$.

It is interesting to point out that the orthogonal transformation $\boldsymbol{R}_1(\theta)$ and the unitary transformation $\boldsymbol{R}_2(\varphi)$ are related to the normalized circular-pol correlation coefficients proposed by Ainsworth *et al.* [8] which are used to characterize man-made structures in urban areas. Here the transformation angle θ and φ respectively account for the orientation angle and helicity in their paper. This again explains that distinction of man-made structures can be improved by such a double transformation.

One last comment on the orthogonal/unitary transformation is that they do not change the coherency matrix of the volume scattering as long as it is modeled as a diagonal matrix with equal second and third diagonal elements as is shown in Equation (12) in the next section. This legitimates estimating the volume scattering power from the transformed matrix if reflection symmetry and uniformly distributed random scatterers are assumed. For simplicity, we denote $\boldsymbol{T}' = \boldsymbol{T}(\varphi)$ which will be hereafter used for power decomposition.

3. Adaptive Volume Scattering Model and Power Decomposition

The volume scattering is originally modeled by a cloud of uniformly distributed dipoles [1] whose coherency matrix is given by:

$$\boldsymbol{T}_{\mathrm{V}} = \begin{bmatrix} 2 & 0 & 0 \\ 0 & 1 & 0 \\ 0 & 0 & 1 \end{bmatrix}. \tag{11}$$

However, it has been observed that this model sometimes leads to over-estimation of the volume scattering power and consequently generates a negative power in the derived surface and double-bounce scattering [3]. This phenomenon happens whenever $T'_{11} < 2T'_{33}$ in the transformed coherency matrix. In order to prevent such a problem, we relax the volume scattering model as follows:

$$\boldsymbol{T}_{\mathrm{V}}(\gamma) = \begin{bmatrix} \gamma & 0 & 0 \\ 0 & 1 & 0 \\ 0 & 0 & 1 \end{bmatrix}, 0 \le \gamma \le 2. \tag{12}$$

Equation (12) is able to represent a range of existing volume scattering models by introducing the adaptive parameter γ. For example, when $\gamma = 2$, then it denotes a cloud of dipoles [1]; when $\gamma = 1$, then it is the maximum randomness model proposed by An *et al.* [3]; when $\gamma = 0$, it becomes the extended volume scattering model for urban areas [9] (except for a different scatterer orientation distribution).

The parameter γ can be adaptively determined by choosing the best fit of the volume scattering to the observed data. Specifically, we employ the concept of a similarity parameter proposed in [10]. Mathematically the optimization problem is modeled as:

$$\gamma^* = \arg \max_{0 \le \gamma \le 2} \left\{ \frac{|\langle \boldsymbol{T}', \boldsymbol{T}_{\mathrm{V}}(\gamma) \rangle|}{\|\boldsymbol{T}'\| \|\boldsymbol{T}_{\mathrm{V}}(\gamma)\|} \right\}. \tag{13}$$

The reason why the similarity parameter is chosen is that it offers the most natural way to compare two matrices. In fact, it represents the inner product of the vector space spanned by 3×3 Hermitian matrices. If we define the inner product of two Hermitian matrices $\boldsymbol{A}$ and $\boldsymbol{B}$ as $\mathrm{Tr}(\boldsymbol{A}^H \boldsymbol{B})$ where $\mathrm{Tr}(.)$ denotes the trace, then it is easy to derive the solution of Equation (13) as follows:

$$T'_{11} < T'_{22} + T'_{33} \Rightarrow \gamma^* = \frac{2T'_{11}}{T'_{22} + T'_{33}}, \tag{14a}$$

$$T'_{11} > T'_{22} + T'_{33} \Rightarrow \gamma^* = 2. \tag{14b}$$

After γ^* has been determined, the remaining procedure is the same to that of the Freeman-Durden decomposition [1]. However, it can be shown that as a consequence of the adaptive volume model Equation (14), the negative power problem will be completely avoided. After subtracting the volume scattering from $\boldsymbol{T}'$, the remaining coherency matrix becomes:

$$\boldsymbol{T}_{\mathrm{SD}} = \boldsymbol{T}' - T'_{33} \boldsymbol{T}_{\mathrm{V}}(\gamma^*) = \begin{bmatrix} T'_{11} - \gamma^* T'_{33} & T'_{12} & 0 \\ (T'_{12})^* & T'_{22} - T'_{33} & 0 \\ 0 & 0 & 0 \end{bmatrix}. \tag{15}$$

Note, in Equation (15) $T'_{22} - T'_{33} > 0$ always holds as a result of the double transformation introduced in Section 2. It is also easy to verify that $T'_{11} - \gamma^* T'_{33} > 0$ as a result of Equation (14). In other words, both diagonal elements remain positive, which prevents any possible negative solutions.

Still, positivity in the diagonal elements does not always guarantee a solution when equating the remaining coherency matrix to the weighted sum of surface and double-bounce models, that is:

$$\boldsymbol{T}_{SD} = f_S \boldsymbol{T}_S + f_D \boldsymbol{T}_D = f_S \begin{bmatrix} 1 & \beta & 0 \\ \beta^* & |\beta|^2 & 0 \\ 0 & 0 & 0 \end{bmatrix} + f_D \begin{bmatrix} |\alpha|^2 & \alpha & 0 \\ \alpha^* & 1 & 0 \\ 0 & 0 & 0 \end{bmatrix}, |\alpha| < 1, |\beta| < 1, \tag{16}$$

where f_S, f_D, α, and β are unknowns to be determined. According to Equations (15) and (16), one needs to solve the following equations:

$$f_S + f_D |\alpha|^2 = T'_{11} - \gamma^* T'_{33}, \tag{17a}$$

$$f_S |\beta|^2 + f_D = T'_{22} - T'_{33}, \tag{17b}$$

$$f_S \beta + f_D \alpha = T'_{12}. \tag{17c}$$

Whether a solution exists to Equation (17) depends on the relationship between $\left(T'_{11} - \gamma^* T'_{33}\right)$ $\left(T'_{11} - T'_{33}\right)$ and $\left|T'_{12}\right|^2$. If $\left(T'_{11} - \gamma^* T'_{33}\right)\left(T'_{11} - T'_{33}\right) \geq \left|T'_{12}\right|^2$, then at least one physically meaningful (non-negative power) solution exists to Equation (17). In fact, the common treatment by assuming there is a dominant scattering mechanism [1] gives one a reasonable result. Another solution can be also derived by the eigen-decomposition approach [4].

However, if $\left(T'_{11} - \gamma^* T'_{33}\right)\left(T'_{11} - T'_{33}\right) < \left|T'_{12}\right|^2$, it can be proved that no solution to Equation (17) exists (Appendix 1). In this case, f_S, f_D, α, and β are found by:

$$\min_{f_S, f_D, \alpha, \beta} \{|f_S \beta + f_D \alpha - T'_{12}|\}$$
$$\text{subject to: } f_S + f_D |\alpha|^2 = T'_{11} - \gamma^* T'_{33}, f_S |\beta|^2 + f_D = T'_{22} - T'_{33}. \tag{18}$$

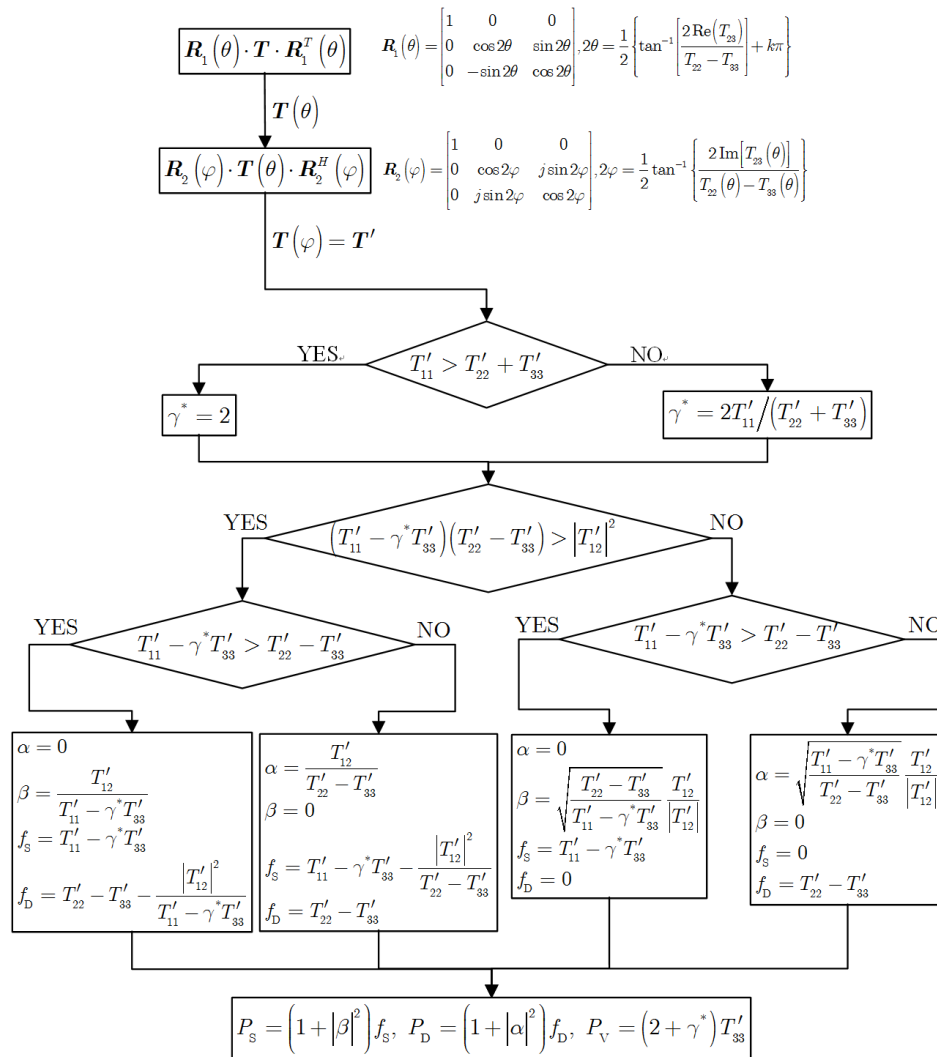The solution of the above problem is as follows (Appendix 1):

$$T'_{11} - \gamma^* T'_{33} > T'_{22} - T'_{33} \Rightarrow f_S = T'_{11} - \gamma^* T'_{33}, f_D = 0, \beta = \sqrt{\frac{T'_{22} - T'_{33}}{T'_{11} - \gamma^* T'_{33}}} \frac{T'_{12}}{|T'_{12}|}, \tag{19a}$$

$$T'_{11} - \gamma^* T'_{33} < T'_{22} - T'_{33} \Rightarrow f_S = 0, f_D = T'_{22} - T'_{33}, \beta = \sqrt{\frac{T'_{11} - \gamma^* T'_{33}}{T'_{22} - T'_{33}}} \frac{T'_{12}}{|T'_{12}|}. \tag{19b}$$

Note that in Equation (19a) the value of α has no significance because the double-bounce scattering does not contribute to the total power ($f_D = 0$) and *vice versa*.

To sum up, the entire procedure for decomposing the PolSAR data using the adaptive volume scattering models is illustrated by the flowchart in Figure 1.

Figure 1. Flowchart of three-component power decomposition with adaptive volume scattering model.

4. Experimental Results

A C-band PolSAR image acquired by the NASA/JPL (National Aeronautics and Space Administration/Jet Propulsion Laboratory) Airborne SAR (AIRSAR) is selected for testing the proposed method. The image is originally multi-look processed but further spatial multi-looking is performed by combining 2×2 (range $\times$ azimuth) neighboring pixels in order to suppress the speckle effect. The image scene is primarily covered by forested areas which can be used for validating the volume scattering model. Figure 2(a) displays the color-coded decomposition image with a fixed volume scattering model of Equation (11) and Figure 2(b) is the color-coded decomposition image with the adaptive volume scattering model of (12). Furthermore, Figure 2(c) shows the map of γ in the adaptive volume scattering model for each pixel. It can be seen that in most of the forested area, γ is equal or near to the theoretical value of 2. For example, the averaged volume scattering model within the selected rectangle in Figure 2(c) is:

$$\overline{T}_{\mathrm{V}} \approx \begin{bmatrix} 1.95 & 0 & 0 \\ 0 & 1 & 0 \\ 0 & 0 & 1 \end{bmatrix}. \tag{20}$$

This is very close to the original model of Equation (11) which prevents volume scattering from being under-estimated in vegetated areas. In order to examine the results quantitatively, the power distributions of Figure 2(a,b) in the same selected patches are shown in Figure 3. It can be seen that in the vegetated area, using the fixed volume scattering model and the adaptive scattering model produce very similar results. However, for man-made structures, as indicated by the arrows in Figure 2, γ is much lower than 2, indicating the volume scattering is significantly reduced so that the surface and double-bounce scattering are enhanced. Moreover, while the decomposition result with the fixed volume scattering model produces negative powers for 18,965 pixels out of a total of 327,168 pixels, the proposed method gives positive solutions all over the image.

Figure 2. (**a**) Original Freeman-Durden decomposition result for AIRSAR data; (**b**) Proposed adaptive decomposition result for AIRSAR data; (**c**) Map of γ.
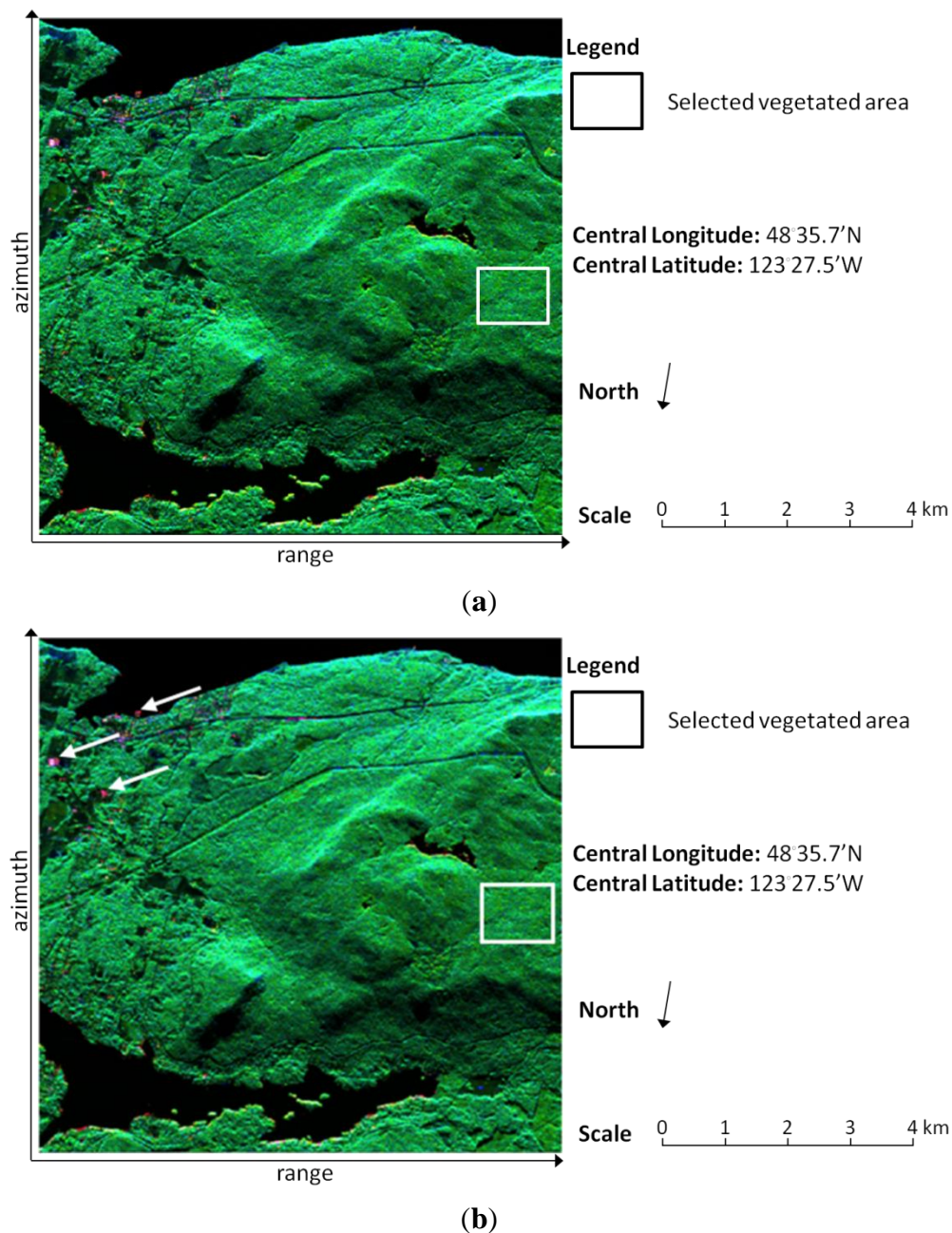

(**a**)
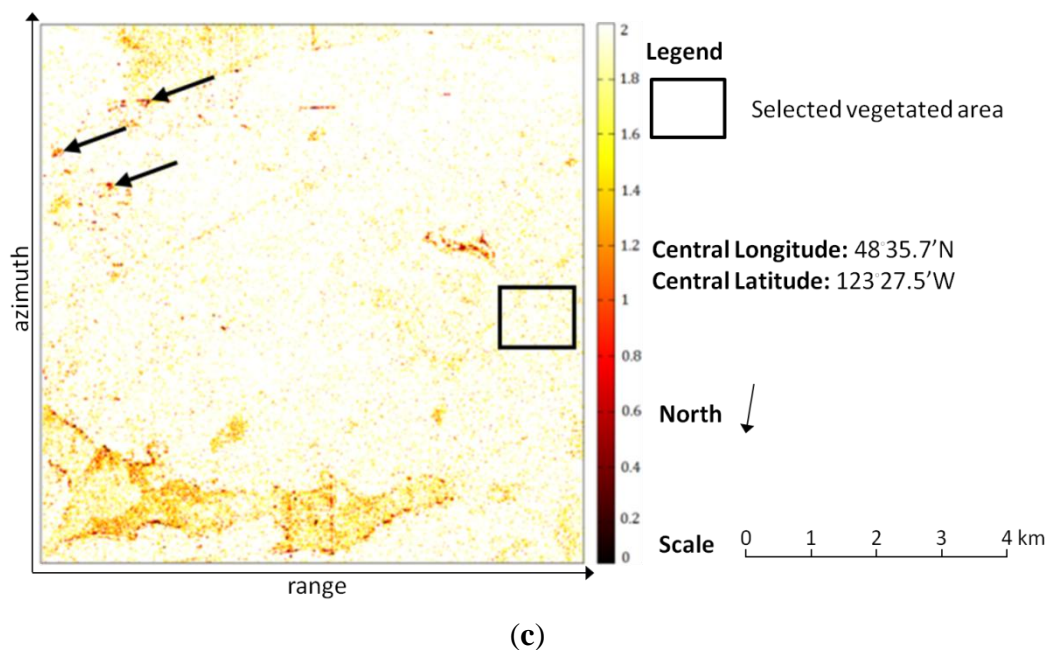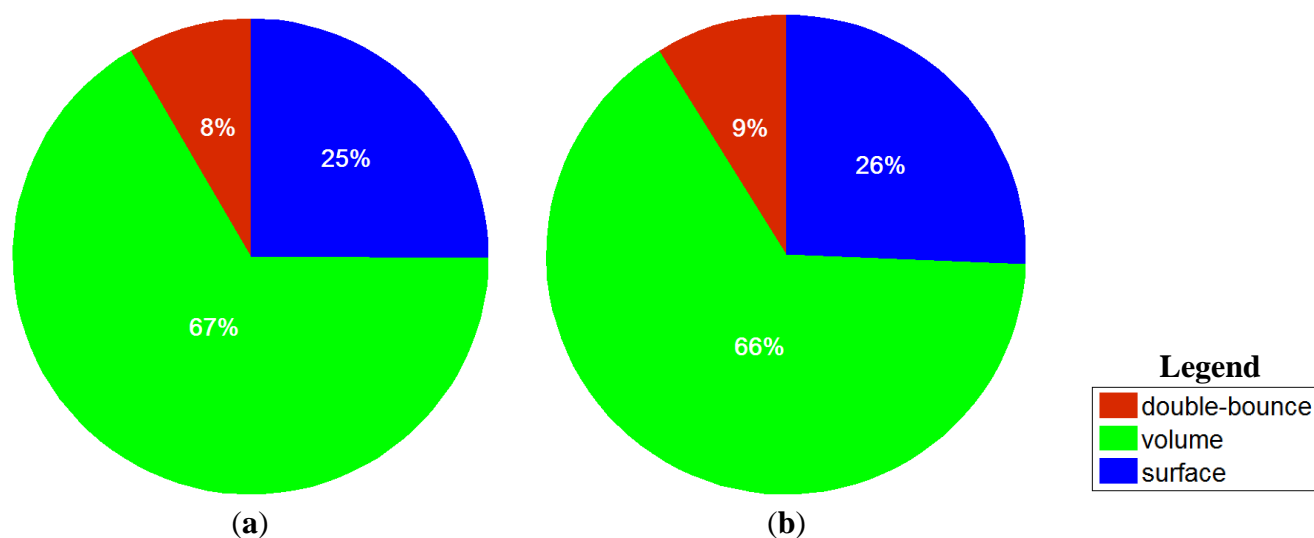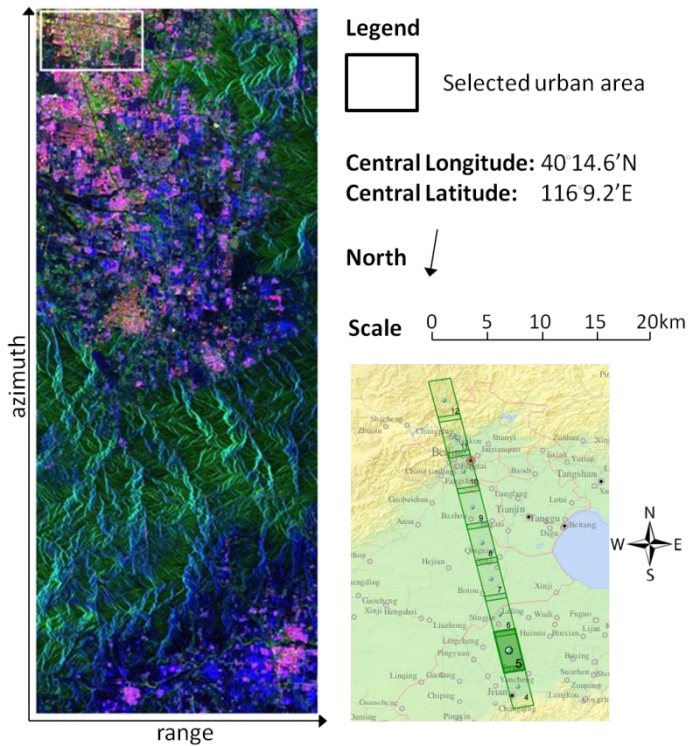

(**b**)

Figure 2. *Cont.*

(**c**)

Figure 3. (**a**) Power distribution of original Freeman-Durden decomposition in vegetated area; (**b**) Power distribution of proposed adaptive decomposition in vegetated area.
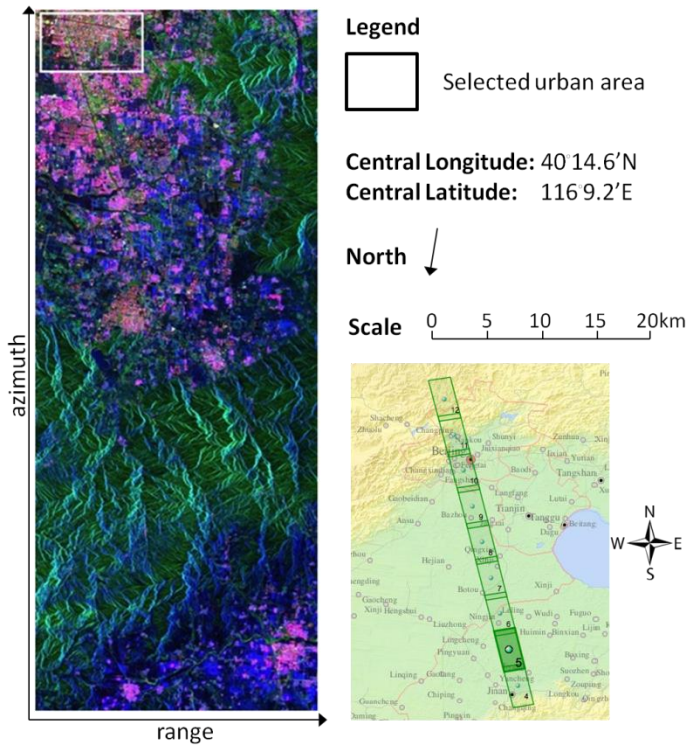

(**a**)   (**b**)

The ability of the proposed method to improve discrimination of man-made structures is more evident in Figure 4, where a PolSAR image acquired by ALOS-PALSAR over the Beijing suburban area is experimented with. Spatial multi-looking has been performed by combining 12 (azimuth) $\times$ 2 (range) pixels so that square ground spacing is approximately achieved. Again, it can be seen from Figure 4(c) that in the urban area, the parameter γ (and consequently the volume scattering power) is significantly reduced. This phenomenon can be also observed in the upper right corners of both Figure 4(a,b) which are correspondingly zoomed in Figure 5(a,b). Again, we draw the power distributions for the selected urban area and the results are shown in Figure 6. Compared to Figure 3, we can see that the volume scattering power is more suppressed in the urban area than in the vegetated

area by the proposed method. This helps to discriminate manmade structures especially oblique to the radar azimuth direction as in Figure 5.

Figure 4. (**a**) Original Freeman-Durden decomposition result for ALOS-PALSAR data; (**b**) Proposed adaptive decomposition result for ALOS-PALSAR data; (**c**) Map of γ.
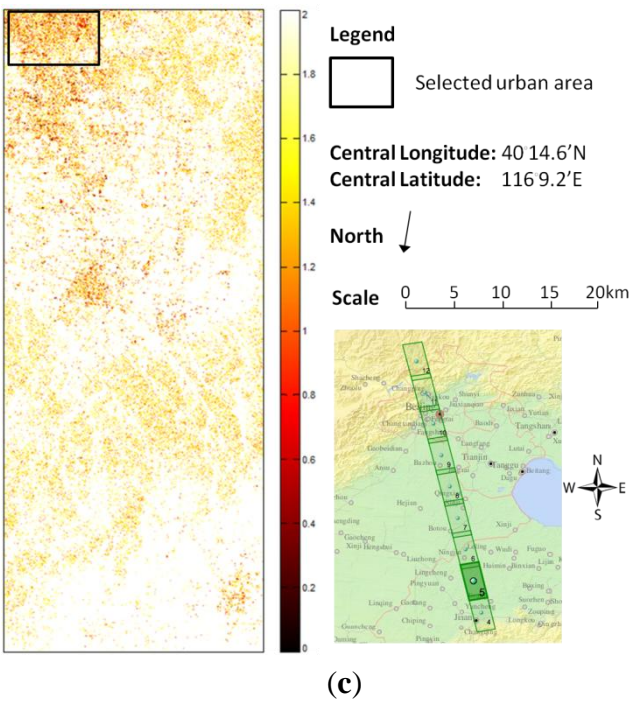

(**a**)

(**b**)

Figure 4. *Cont.*

(**c**)

Figure 5. (**a**) Zoomed result by the original Freeman-Durden decomposition; (**b**) Zoomed result by the proposed adaptive decomposition
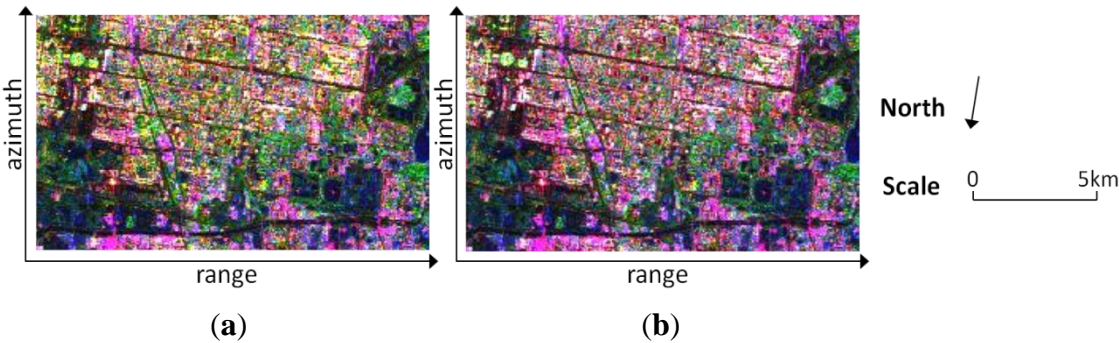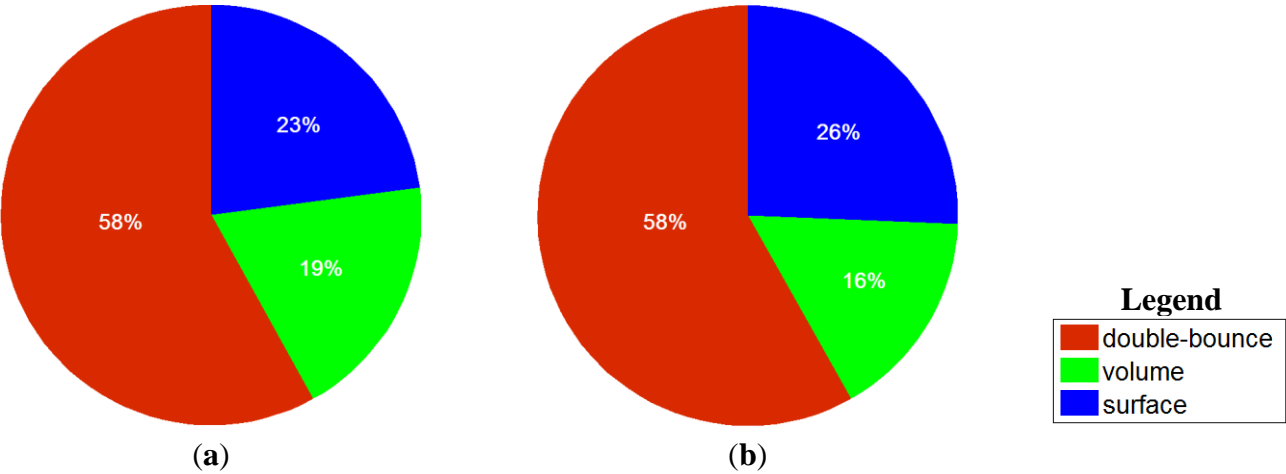

(**a**)   (**b**)

Figure 6. (**a**) Power distribution of original Freeman-Durden decomposition in urban area; (**b**) Power distribution of proposed adaptive decomposition in urban area.

(**a**)   (**b**)

5. Discussion

It is worth noting that the adaptive volume scattering model proposed in this paper is similar to that used by Freeman [11], which can be rewritten in its equivalent coherency matrix form as:

$$\widetilde{T}_{V}(\gamma) = \begin{bmatrix} \gamma & 0 & 0 \\ 0 & 1 & 0 \\ 0 & 0 & 1 \end{bmatrix}, 1 \leq \gamma \leq \infty \tag{21}$$

By comparing Equations (12) and (21), the difference lies in the range for γ. However, Equation (21) cannot be directly used in the three-component decomposition scheme because there exists risk in over-estimating the volume scattering power (note γ can be arbitrarily large by definition). Instead, Freeman proposed to use it in a two-component scattering model for fitting the PolSAR data from forests. In our model, on the other hand, we specifically restrict the upper bound of γ. This is validated by Equation (20) where the averaged volume scattering model in forested areas indeed approximates the maximum theoretical setting. In addition, our model tries to account for the volume scattering mechanism in urban areas by letting $\gamma < 1$, which equivalently indicates that the HH-VV correlation is out of phase, *i.e.*, $\mathrm{Re}(S_{HH}S_{VV}^{*}) < 0$. An explanation of this phenomenon is that the volume scattering within urban areas can be affected by randomly orientated double-bounce scatterers. Our experiments showed that discrimination of urban areas is improved by such an assumption.

6. Conclusion

In this paper, we have proposed an adaptive three-component power decomposition method for PolSAR data. This method modifies the original Freeman-Durden decomposition [1] by adopting an adaptive volume scattering model. Although our adaptive model takes a similar form to that in [11], there exist significant distinctions including the range of the adaptive parameter as well as the decomposition methodology. In [11], the adaptive volume scattering model is fitted under a two-component decomposition scheme where the adaptive parameter is derived by solving established equations; while in our method the adaptive parameter is derived by solving an optimization problem thanks to the use of a similarity parameter [10]. This treatment enables us to incorporate the adaptive volume scattering model into the three-component decomposition scheme and the increased methodological complexity is negligible.

Experimental results demonstrate that, compared with the original Freeman-Durden decomposition with the fixed volume scattering model, the proposed method produces similar/better decomposition results in vegetated areas, but on the other hand is able to improve discrimination in urban regions. In addition, the proposed method always produces non-negative powers and the power sum of all components equals the total power. This is done with mathematical rigor rather than in an *ad-hoc* fashion so that further quantitative analysis can be reliably conducted based on the decomposition result.

References

1. Freeman, A.; Durden, S.L. A three-component scattering model for polarimetric SAR data. *IEEE Trans. Geosci. Remote Sens.* **1998**, *36*, 963–973.
2. Yamaguchi, Y.; Moriyama, T.; Ishido, M.; Yamada, H. Four-component scattering model for polarimetric SAR image decomposition. *IEEE Trans. Geosci. Remote Sens.* **2005**, *43*, 1699–1706.
3. An, W.; Cui, Y.; Yang, J. Three-component model-based decomposition for polarimetric SAR data. *IEEE Trans. Geosci. Remote Sens.* **2010**, *48*, 2732–2739.
4. Van Zyl, J.J.; Arii, M.; Kim, Y. Model-based decomposition of polarimetric SAR covariance matrices constrained for nonnegative eigenvalues. *IEEE Trans. Geosci. Remote Sens.* **2011**, *49*, 1104–1113.
5. Arii, M.; Van Zyl, J.J.; Kim, Y. Adaptive model-based decomposition of polarimetric SAR covariance matrices. *IEEE Trans. Geosci. Remote Sens.* **2011**, *49*, 1104–1113.
6. Singh, G.; Yamaguchi, Y.; Park, S.-E. 4-Component Scattering Power Decomposition with Phase Rotation of Coherency Matrix. In *Proceedings of 2011 IEEE International Geoscience and Remote Sensing Symposium*, Vancouver, BC, Canada, 25–29 July 2011.
7. Yamaguchi, Y.; Sato, A.; Boerner, W.M.; Sato, R.; Yamada, H. Four-component scattering power decomposition with rotation of coherency matrix. *IEEE Trans. Geosci. Remote Sens.* **2011**, *49*, 2251–2258.
8. Ainsworth, T.L.; Schuler, D.L.; Lee, J.-S. Polarimetric SAR characterization of man-made structures in urban areas using normalized circular-pol correlation coefficients. *Remote. Sens. Environ*. **2008**, *112*, 2876–2885.
9. Sato, A.; Yamaguchi, Y.; Singh, G.; Park, S.-E. Four-component scattering power decomposition with extended volume scattering model. *IEEE Geosci. Remote Sens. Lett*. **2012**, *9*, 166–170.
10. An, W.; Zhang, W.-J.; Yang, J.; Hong, W.; Cao, F. On the similarity parameter between two targets for the case of multi-look polarimetric SAR. *Chin. J. Electron*. **2009**, *18*, 545–550.
11. Freeman, A. Fitting a two-component scattering model to polarimetric SAR data from forests. *IEEE Trans. Geosci. Remote Sens.* **2007**, *45*, 2583–2592.

Appendix

We first prove that if $\left(T_{11}' - \gamma^* T_{33}'\right)\left(T_{11}' - T_{33}'\right) < \left|T_{12}'\right|^2$, then there exists no solution to Equation (17). Specifically, we prove that if Equations (17a) and (17b) hold, Equation (17c) will be not satisfied. According to Cauchy-Schwarz inequality, we have:

$$|f_S\beta + f_D\alpha|^2 \leq (f_S + f_D|\alpha|^2)(f_D + f_S|\beta|^2) = (T_{11}' - \gamma^* T_{33}')(T_{22}' - T_{33}') < |T_{12}'|^2 \qquad \text{(A1)}$$

Equation (A1) shows that for any f_S, f_D, α, and β, $|f_S\beta + f_D\alpha| < \left|T_{12}'\right|$, which contradicts Equation (17c). Thus no solution to Equation (17) can be found.

Next we solve the problem of Equation (18) under $\left(T_{11}' - \gamma^* T_{33}'\right)\left(T_{11}' - T_{33}'\right) < \left|T_{12}'\right|^2$. According to the triangular inequality and Equation (A1), we have:

$$|f_S\beta + f_D\alpha - T_{12}'| \geq |T_{12}'| - |f_S\beta + f_D\alpha| \geq |T_{12}'| - \sqrt{(T_{11}' - \gamma^* T_{33}')(T_{22}' - T_{33}')} \qquad \text{(A2)}$$

The above equality holds if and only if:

$$f_S \beta + f_D \alpha = k T'_{12} \tag{A3a}$$

$$f_S |\beta|^2 = \delta f_S \tag{A3b}$$

$$f_D = \delta f_D |\alpha|^2 \tag{A3c}$$

where $k, \delta > 0$ are the proportional constants. Substituting Equations (A3b) and (A3c) into the equation constraints of Equation (18), we have:

$$\delta = \frac{T'_{11} - \gamma^* T'_{33}}{T'_{22} - T'_{33}} \tag{A4}$$

If $\delta < 1$, note that $|\alpha| < 1$, then according to Equation (A3c) $f_D = 0$; on the other hand, if $\delta > 1$, note that $|\beta| < 1$, according to Equation (A3b) $f_S = 0$. The rest of the procedure is straightforward and the final result is given in Equation (19).